Nuclear Science and Techniques (2025) 36:178
https://doi.org/10.1007/s41365-025-01754-9

Experimental extraction of neutron resonance parameters at 20–300 eV for ^{147,149}Sm

Xin-Xiang Li[1] · Long-Xiang Liu[2] · Wei Jiang[3,4] · Ya-Ju Chen[1] · Jie Ren[5] · Hong-Wei Wang[2,6] · Gong-Tao Fan[2,6] · Wen Luo[1] · Song Feng[1] · Wen Xie[1] · Zi-Ang Lin[1] · Ting Jiang[1] · Gao-Le Yang[7] · Zhen-Dong An[8] · Xian-Kai Li[1,7] · Zhou-Ji Liao[1] · Jie-Ming Xue[9] · Xin-Yu Li[10] · Ning-Xin Peng[1] · De-Xin Wang[11] · Su-Ya-La-Tu Zhang[11] · Yue Zhang[2] · Xin-Rong Hu[12] · Zi-Rui Hao[2] · Bing Jiang[3,4] · Xiao-He Wang[13] · Ji-Feng Hu[13] · Ying-Du Liu[14] · Chun-Wang Ma[15,16] · Yu-Ting Wang[15] · Jian-Jun He[17] · Li-Yong Zhang[18,19]

Received: 4 November 2024 / Revised: 27 January 2025 / Accepted: 19 February 2025 / Published online: 17 July 2025

Abstract

^{147,149}Sm are slow neutron capture (s-process) nuclides in nuclear astrophysics, whose (n,γ) cross sections are important input parameters in nucleosynthesis network calculations in the samarium (Sm) region. In addition, ^{149}Sm is a fission product of ^{235}U with a 1% yield, and its neutron resonance parameters play a critical role in reactor neutronics. According to the available nuclear evaluation databases, a significant disagreement has been observed in the resonance peaks of the ^{147,149}Sm (n,γ) cross-sectional data within the energy range of 20–300 eV. In this study, tutron capture cross section of a natural samarium target was measured at the back-streaming white neutron beamline of the China Spallation Neutron Source. The neutron capture yield was obtained, and the neutron resonance parameters for ^{147}Sm at 107.0, 139.4, 241.7, and 257.3 eV and ^{149}Sm at 23.2, 24.6, 26.1, 28.0, 51.5, 75.2, 90.9, 125.3, and 248.4 eV were extracted using the SAMMY code based on R-matrix theory. For the parameters Γ_n and Γ_γ in these energies of ^{147,149}Sm, the percentages consistent with the results of the CENDL-3.2, ENDF/B-VIII.0, JEFF-3.3, JENDL-4.0, and BROND-3.1 database are 27%, 65%, 65%, 42%, and 58%, respectively. However, 27% of the results were inconsistent with those of the major libraries. This work enriches experimental data of the ^{147,149}Sm neutron capture resonance and helps clarify the differences between different evaluation databases at the above energies.

Keywords Neutron capture cross section · Neutron resonance parameters · Back-n facility

1 Introduction

Super-iron elements originate from the current focal points in nuclear astrophysics. Over 98% of heavy elements are formed through the slow neutron capture process (*s* process) [1] and fast neutron capture process (*r* process) [2]. However, certain stable nuclides cannot be produced by either the *s* or *r* processes, containing more protons and separated from *s* and *r* nuclei by unstable isotopes between ^{74}Se and ^{194}Hg, collectively known as p-nuclei, with "p" representing proton- rich nuclides, totaling 35 nuclei in all [3]. Despite their rarity and low abundance, the synthesis of p-nuclei involves a wide range of nuclei. Therefore, it is crucial to investigate the P-process mechanism to gain a comprehensive understanding of nucleosynthesis. Cross-sectional and structural studies of these 35 p-nuclei provided valuable insights into the p-process mechanism. To gain a more precise understanding of celestial nuclear processes and related element synthesis, it is essential to study the nuclear mass, reaction cross section, and decay properties [4].

Natural Sm consists of eight stable isotopes, with ^{147,149}Sm synthesized using the *s* process. Among these isotopes, ^{149}Sm is exclusively produced by the *s* process because its stable neodymium isobars shield it from the contributions of the *r* process. The (n,γ) cross-sectional data for

This work was supported by the Natural Science Foundation of Hunan Province, China (No. 2025JJ60020), the National Key Research and Development Program (No. 2022YFA1603300) and National Natural Science Foundation of China (Nos.12275338 and 12388102). China Institute of Atomic Energy (No. CIAE-FW-GKJT-23-0820).

Extended author information available on the last page of the article

these isotopes provide valuable insights into the nucleosynthesis pathway in the samarium region. Furthermore, ^{235}U is an important raw material for nuclear reactors [5]. As the operation of a nuclear reactor progresses, a multitude of fission-product nuclides are inevitably produced from the fission of fissile materials, such as ^{235}U, some of which exhibit significantly high thermal neutron absorption cross sections. Among these fission products, ^{149}Sm, with a 1% yield from ^{235}U fission, plays an important role in reactor neutronics because of its neutron capture cross section [6].

According to available nuclear evaluation databases such as ENDF B-VIII.0, CENDL-3.2, JENDL-4.0, JEFF-3.3, and BROND-3.1, significant deviations were observed in the resonance peaks of the ^{nat}Sm (n,γ) cross-section data within the energy range of 1–300 eV. Figure 1 illustrates the deviation in neutron capture reaction data for ^{149}Sm as reported in different evaluation databases compared to the ENDF/B-VIII.0 database. The deviation is calculated by $|\sigma_i - \sigma|/\sigma$ (i =1,2,3...), where σ is the ^{149}Sm (n,γ) cross section in ENDF/B-VIII.0 database and σ_i is from the other evaluated databases. As shown in Fig. 1, in the energy range between 1 and 300 eV, the cross section of ^{149}Sm (n,γ) in most evaluation databases differs from ENDF/B-VIII.0, with the deviation in the CENDL-3.2 and JENDL-5 databases reaching or exceeding 100%. As indicated by the available Experimental Nuclear Reaction Data (EXFOR), no experimental data can clarify the differences between the evaluation databases mentioned above.

The China Spallation Neutron Source (CSNS) is a large-scale multidisciplinary application platform based on high-power proton accelerators and is primarily utilized for material structure research through neutron-scattering technology [7]. The CSNS accelerator comprises a 80 MeV hydrogen-negative-ion linear accelerator, a fast-cycle proton synchrotron accelerator with an energy of 1.6 GeV, and two proton beam transport lines [8]. The proton beam energy provided at the CSNS was 1.6 GeV, with a beam power of 100 kW(now in 180 kW) and a repetition frequency of 25 Hz. Tungsten targets of varying thicknesses were employed for the scattering reaction with protons, each wrapped in tantalum with a thickness of 0.5 mm and separated by cooling water layers measuring 1.5 mm [9, 10]. Upon impact of the proton beam on the tungsten target, the estimated neutron flux can reach 2.0×10^{16}cm^{-2}s^{-1} [11–16].

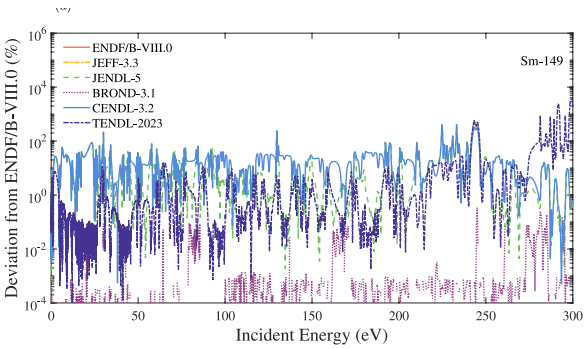

Fig. 1 (Color online) The deviation in neutron capture reaction data for ^{149}Sm, as reported in different evaluation databases, compared to the ENDF/B-VIII.0 database

In this study, the neutron capture cross section of natural samarium was within the energy range of 20–300 eV at the back-streaming white neutron (Back-n) facility at the CSNS [17–22]. The ^{nat}Sm experiment was conducted in 2019, and a method that integrates a Monte Carlo simulation to ascertain the in-beam γ-ray background [23] was subsequently utilized to analyze samarium neutron capture cross-section data. The resonance parameters for each isotope within this energy range were derived using the SAMMY software. The experimental results clarified the differences in the ^{147,149}Sm neutron resonance parameters in different evaluation databases under specific energies, for example, at 139.4 eV. The neutron resonance parameters Γ_n of the ^{147}Sm isotope in the database of CENDL-3.2 and JENDL-4.0 are 69.1 meV, which is different from the ENDF/B-VIII.0, JEFF-3.3, and BROND-3.1 databases; the values in these databases are uniformly 88 meV. The results of this study were 89.0 ± 8.8 meV. Additional results and detailed analyses are presented below.

2 Method and material

2.1 Experimental setup

A neutron capture experiment was conducted at end station 2 (ES#2) of the back-n beamline. The measurement utilized a detection system consisting of four C_6D_6 scintillation detectors, each with a diameter of 127 mm and length of 76.2 mm, housed within a 1.5-mm-thick aluminum capsule, and coupled with a photomultiplier tube (ETEL 930 KEB PMT). For the measurement of the neutron capture reaction cross section, the C_6D_6 detector offers several advantages [24]: (1) It exhibits low sensitivity to neutrons, which is crucial for eliminating background signals in the detection of the final state γ rays from the (n,γ) reaction. This insensitivity significantly reduces the neutron-induced background. (2) The C_6D_6 detector demonstrates a fast time response, with signal responses to neutrons and γ-rays on the order of nanoseconds. Coupled with the response time of the photomultiplier tube, this resulted in a rise time of approximately 10 ns for the entire anode signal, thereby improving the overall time resolution of the detection systems. (3) Through pulse-height weighting technique (PHWT), the detection efficiency of C_6D_6 detectors can be independent of decay paths, multiplicity, and energy distribution of γ rays.

The physical arrangement and Monte Carlo simulation reconstruction of the detector system and target are presented in Refs. [25], with the detailed layout parameters provided in Ref.[26]. The detector was placed opposite to the direction of the beam. This configuration minimizes the background interference from beam scattering, given that γ-rays emitted by neutron capture reactions are isotropic. The neutron flux was determined using a Li-Si detector based on the ^{6}Li(n,α)^{3}H reaction. The energy spectra were obtained from back-n collaboration, with an uncertainty of less than 8.0% for $E_n < 0.15$ MeV [27]. The Back-n data acquisition system (DAQ) employs a full-waveform data acquisition solution.

In this study, the TOF () method was used to determine the resonance energy of the neutrons. E_n is expressed as follows:

$$E_n = \frac{1}{2} m_n \left(\frac{L}{t_n} \right)^2, \tag{1}$$

where m_n is the neutron mass, L is the flight distance, and t_n is the flight time. In the Back-n facility, t_n is determined as $t_n = (t_{det} - t_\gamma) + \frac{L}{c}$, where t_{det} is the time when the detector responds to neutrons or γ rays, t_γ is the time when the γ flash arrives at the detector, and c is the speed of light [28]. ES#2 is approximately 76 m from the spallation target, and the value of L is 77.26 m in our case. The uncertainty in L is mainly caused by multiple scattering of neutrons inside the spallation target [29].

In the normal operating mode of a CSNS, there are two proton bunches with a time interval of 410 ns for each pulse, which has a repetition frequency of 25 Hz. Because of the superposition of the event distributions corresponding to the two bunches, the resolution of the TOF measurement at back-n is degraded by the double-bunch characteristics if the measured event distribution is used directly without unfolding, particularly in the higher neutron energy region [30]. In this study, we used the analytical method developed by the back-n collaboration to nearly recover the event distribution corresponding to a single proton bunch [31].

The experiment was conducted in May 2019 and involved the preparation of gold (^{197}Au), carbon (^{nat}C), empty, and natural samarium (^{nat}Sm) targets. A total beam time of approximately 49 h was used in this study. The ^{197}Au(n,γ)^{198}Au reaction, serving as a standard neutron capture cross section, was initially measured for 13 h at proton power levels ranging from 50.5–51.9 kW to validate previous findings [25], thereby ensuring the integrity of the experimental setup and data acquisition (DAQ). Subsequently, measurements were performed on the carbon and empty targets for 12 h and 8 h, respectively, to assess the neutron-scattering background and environmental interference under beam conditions. Throughout this period, the accelerator exhibited relatively stable performance with a beam power of approximately 50 kW and an uncertainty level below 2%. Finally, the natural samarium target was measured for 16 h at beam power levels between 48.3 and 50.5 kW. Details regarding the target parameters and measurement conditions are presented in Table 1, with diameter measurements obtained using Vernier calipers and the thickness determined by micrometer readings.

2.2 Weighting function

The essence of data analysis is to obtain the counts of neutron capture reactions within the target, which are contingent on the detection efficiency and accuracy of the response of the detector to (n,γ) reactions. The efficacy of C_6D_6 scintillators in detecting prompt γ-ray cascades emitted during neutron capture reactions is contingent on the intricate de-excitation path of the compound nucleus. Consequently, it is imperative that the measured signals undergo the pulse-height weighting technique (PHWT), which renders the detection efficiency independent of the cascade γ-ray energies.

Typically, a high detection efficiency is sought after; however, for neutron capture reactions, a low detection efficiency is preferred owing to the phenomenon of γ radiation cascade emission. In the case of neutron capture cascade emission, it is desirable to detect at most one γ ray in the cascade emission, making a low detection efficiency more suitable. Therefore, the detection efficiency of the

Table 1 Information of experimental targets

Target	Impurities			Diameter (mm)	Thickness (mm)	Beam power (kW)
^{nat}Sm	ω(Mo) = 0.002%	ω(Ti) = 0.002%	ω(Tb) = 0.001%	50.00 ± 0.02	1.000 ± 0.005	49.37 ± 1.08
	ω(Fe) = 0.01%	ω(Ca) = 0.005%	ω(C) = 0.01%			
	ω(Si) = 0.01%	ω(Mg) = 0.005%	ω(Nb) = 0.002%			
	ω(Al) = 0.005%	ω(Cl) = 0.005%	ω(Ta) = 0.002%			
	ω(La) = 0.001%	ω(Ce) = 0.001%	ω(Pr) = 0.002%			
^{nat}C	< 0.100%			50.00 ± 0.02	1.000 ± 0.005	50.00 ± 1.00
^{197}Au	< 0.100%			30.00 ± 0.02	1.000 ± 0.005	51.20 ± 0.70

capture reaction is approximately equal to the sum of the detection efficiencies of the capture reaction cascade γ.

$$\varepsilon_c = 1 - \prod(1 - \varepsilon_{\gamma i}) \approx \sum \varepsilon_{\gamma i}, \tag{2}$$

where ε_c is the detection efficiency of the C_6D_6 detector for the capture reaction, and $\varepsilon_{\gamma i}$ is the detection efficiency of the i^{th} cascade γ ray. Because $\varepsilon_{\gamma i}$ is sufficiently small, the equal sign of the above formula holds. Equation (2) establishes the relationship between ε_c and $\varepsilon_{\gamma i}$, but it cannot be directly reflected in the output energy spectrum of C_6D_6 detector. We hope to establish a direct relationship between ε_c and the output energy spectrum of the detector, which is helpful to directly analyze ε_c from the output signal of the detector and then calculate the neutron capture cross section. If the γ detection efficiency in equation (2) is proportional to the γ energy E_γ, then

$$\varepsilon_{\gamma i} = \alpha E_{\gamma i}. \tag{3}$$

Then,

$$\varepsilon_c = \alpha \sum E_{\gamma i}, \tag{4}$$

where α is the scale coefficient and E_γ is the energy of cascade γ, which can be obtained directly from the pulse-height spectrum output by C_6D_6.

For equation (4) to hold, it is necessary to perform mathematical control on the response function of the detection system to realize the relation in (3), which is a pulse-height weighting technique (PHWT). The PHWT was first proposed by Macklin and Gibbons and applied to the C_6F_6 detector to measure the neutron capture cross section [32]. We anticipate that the energy of each group of cascaded γ-rays will be directly proportional to the weighted detection efficiency. The normalized detection efficiency manifests intuitively in the pulse-height spectrum (PH spectrum) counts. Consequently, the detection efficiency of the detector for γ can be characterized by analyzing the pulse-height spectrum. By introducing a weighted function number, we ensure that the following equation is satisfied:

$$\int_{EL}^{\infty} R_d(E_d, E_{\gamma j}) W(E_d) \mathrm{d}E_d = \alpha E_{\gamma j}, \tag{5}$$

where the EL is the threshold of PH spectrum; E_d is an energy bin of PH spectrum; $R(E_d, E_{\gamma j})$ is counts of PH spectrum with energy response function in E_d; $W(E_d)$ is the weight factor corresponding to E_d; $E_{\gamma j}$ is the energy of gamma-ray of group j, and here, we set the coefficient $\alpha = 1$.

The experimental capture yields were determined using a weighting function (WF) parameterized as a polynomial function of the γ-ray energy. WF can be expressed as

$$WF(E_d) = \sum_{i=0}^{4} a_i E_d^i, \tag{6}$$

where a_i is the parameters of the WF, which can be determined using the least-squares fit method:

$$\chi^2 = \sum \left(kE_{\gamma j} - \int_{EL}^{\infty} R(E_d, E_{\gamma j}) WF(E_d) \mathrm{d}E_d \right)^2. \tag{7}$$

Each event was weighted by an appropriate WF to ensure that the weighted efficiency of the detector was directly proportional to its excitation energy, as illustrated in Fig. 2. This manipulation of raw data remains valid when the original efficiency is sufficiently low, allowing for the measurement of only one γ-ray per capture event in the C_6D_6 setup [33].

The energy deposition of different monoenergetic γ rays in the C_6D_6 detector layout [23] was simulated using the Geant4 Monte Carlo program [34, 35]. The original efficiency curves are presented in Fig. 2a. Upon applying the weight function to the original efficiency curve, the linear relationship between the detection efficiency and energy is illustrated in Fig. 2b, with the ratio of efficiency to energy in Fig. 2c approaching unity. Below 1.5 MeV, the weighted efficiency does not exhibit proportionality to the energy, necessitating the establishment of a threshold during PH spectrum processing to mitigate any impact from the failure of the weight function.

2.3 Background analysis

To be effective, the WF must be applied to the net pulse-height spectrum. The key to obtaining the net pulse-height spectrum is background deduction. For the neutron capture cross-section measurements with C_6D_6 detectors at back-n, the background composition was as follows [36]:

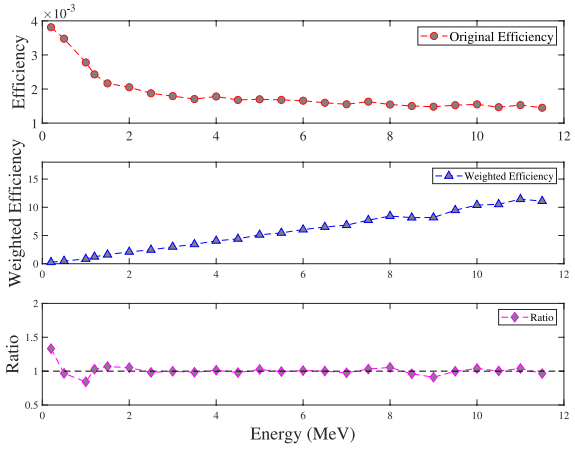

Fig. 2 (Color online) **a** C_6D_6 original efficiency. **b** Weighted efficiency. **c** The ratio of weighted efficiency to γ rays energy

$$B(t) = B_0 + B_{\text{empty}}(t) + B_{\text{sample}}(t), \tag{8}$$

where B_0 is the sample- and time-independent background, $B_{\text{empty}}(t)$ is the time-dependent but sample-independent background, and $B_{\text{sample}}(t)$ is the sample-dependent background, which is related to the scattering of neutrons and γ rays by the sample. The neutron energy E_{n} is derived from the time-of-flight t:

$$B(E_{\text{n}}) = B_0 + B_{\text{empty}}(E_{\text{n}}) + B_{\text{sn}}(E_{\text{n}}) + B_{\text{s}\gamma}(E_{\text{n}}), \tag{9}$$

where B is the total background, which is related to the neutron energy E_{n}; B_{sn} is the background caused by neutron scattering with the target; and $B_{\text{s}\gamma}$ is the background caused by in-beam γ scattering with the target.

The background resulting from environmental activation and delayed γ rays is independent of the sample and time but relies solely on the experimental conditions. In this context, the background is determined by measuring an empty target without a beam to establish B_0. However, the background arising from both the beam and the environment is not influenced by the sample but varies with time. This aspect of the background is assessed by measuring an empty target under the beam conditions to determine $B_{\text{empty}}(E_{\text{n}})$.

The background caused by neutron scattering typically necessitates a target nucleus with a large neutron-scattering cross section in the relevant energy range, while also requiring the neutron capture cross section of the target nucleus to be relatively flat to avoid interfering with the measurement of the Sm target. In this study, we used measurements of the carbon target under beam conditions to determine $B_{\text{sn}}(E_{\text{n}})$. Given its low neutron capture cross section compared to Sm and the absence of a resonance structure in the relevant energy range, lead is an ideal material for evaluating the in-beam γ background $B_{\text{s}\gamma}(E_{\text{n}})$ because of its strong γ-ray scattering capability.

In 2019, we failed to recognize the significance of the in-beam γ background and consequently overlooked this aspect of the data. However, in 2022, we ascertained the general time structure of the in-beam γ background at the back-n facility using various in-beam γ ray experimental findings [23]. Subsequently, we propose a methodology for the comprehensive quantification of in-beam γ rays based on Geant4 simulation. By re-analyzing the 2019 $^{\text{nat}}$Er target experimental results using this approach, we obtained reliable outcomes that validated its efficacy. Furthermore, employing this method, we processed the 2019 $^{\text{nat}}$Sm target experimental data to determine $B_{\text{s}\gamma}(E_{\text{n}})$.

The normalized count spectrum is shown in Fig. 3. The lines $p_0 - p_2$ represent the spectra of the natural samarium, carbon, and empty targets, which were normalized to the neutron flux rate detected by the Li-Si detector. Line p_3 corresponds to the in-beam γ-ray background, and its shape is

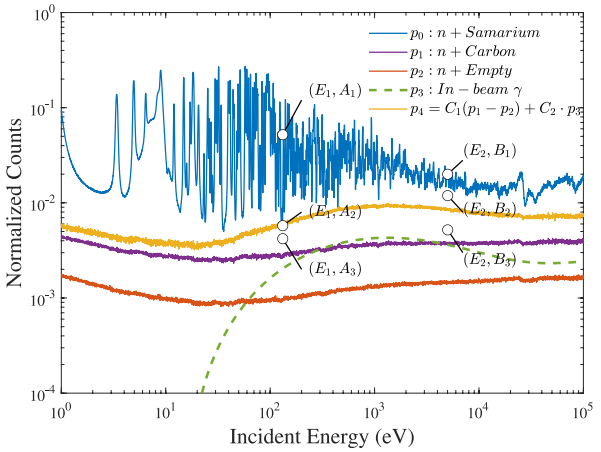

Fig. 3 (Color online) The spectrum of the natural samarium target, empty target, and carbon target (normalized to the neutron flux rate). The in-beam γ ray background is determined by simulation, as described in Ref. [23]

measured using a lead target. As discussed in Ref.[23], there exists a general formula and parameters for expressing its shape at the Back-n facility until significant modifications are made to the beamline that may impact the generation or transportation of in-beam γ rays. We considered the inclusion of a Co filter at the beamline, which exhibits two distinct resonance absorption peaks at energies of $E_1 = 132\,\text{eV}$ and $E_2 = 5.016\,\text{keV}$. When the filter is designed to completely absorb neutrons, only γ rays remain in the beam. Consequently, $A_1(B_1)$ corresponds to line p_0 at an energy of $E_1(E_2)$, representing the result of natural samarium reacting with neutrons and γ rays, whereas $A_2(B_2)$ is obtained through simulation, depicting the outcome of a natural samarium target interacting solely with γ rays.

Let $A_3 = A_2\sigma_1/\sigma_2(B_3 = B_2\sigma_1/\sigma_2)$, where $\sigma_1(\sigma_2)$ is the γ-ray elastic cross section of the lead and $^{\text{nat}}$Sm target. $p_4 = C_1(p_1 - p_2) + C_2 \cdot p_3$. C_1 is the ratio of the neutron-scattering cross section of samarium to that of carbon. Let points (E_1, A_3) and (E_2, B_3) be in line p_4; then, parameter C_2 can be determined.

3 Results and discussion

3.1 Neutron capture yield

The net PH spectrum was derived by subtracting the background values. Following the application of WFs, the capture yield can be determined as follows:

$$Y_{\text{w}}(E_{\text{n}}) = \frac{N_{\text{w}}(E_{\text{n}})}{N_{\text{s}} I(E_{\text{n}}) S_{\text{n}}}, \tag{10}$$

where $Y_w(E_n)$ is the capture yield, $N_w(E_n)$ is the weighted pulse-height spectrum, N_s is the target area density, $I(E_n)$ is the neutron flux measured by Back-n collaboration [27], and S_n is the target neutron separation energy. For a natural Sm target, each resonance corresponds to a specific isotope and possesses its own separation energy for efficient capture. Consequently, the value of S_n varies across the different resonance peaks. The method used to calculate the value of S_n for the ^{nat}Sm target is shown in Fig. 4. Different colors represent different Sm isotopes. Line types (including dotted, solid, and dashed lines) indicate the variations in neutron capture cross sections of isotopes with incident neutron energy, and dot types represent the different values of the neutron separation energy S_n. Both linear and point patterns are presented in Fig. 4 to demonstrate that the value of the natural target S_n is based on the contributions of different isotopes to the resonance peaks. Because S_n ranges from 5.81 MeV (^{154}Sm) to 8.15 MeV (^{147}Sm), no significant difference can be observed on the y-axis scale in Fig. 4, and $S_n \times \max(\sigma)$ is employed to reflect the value of natural target S_n at different energies. The dotted lines in Fig. 4 show that since different isotopes contribute different resonance peaks, the S_n value of the natural target is a piecewise function, which is related to the formant position of different isotopes. The values of S_n for the ^{nat}Sm isotopes can be obtained based on a new atomic mass evaluation(AME2020) [37].

3.2 Uncertainty

The uncertainty in the capture yield encompasses several contributing factors, as outlined in [26]: variability arising from the experimental conditions, data analysis, and statistical error.

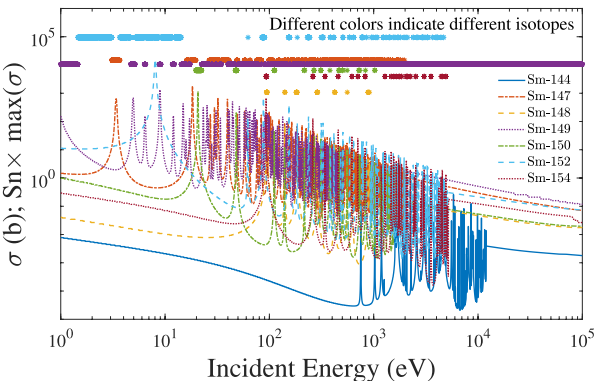

Fig. 4 (Color online) The normalized value of cross section for different isotopes and the value of S_n for natural samarium element. Line types (including dot lines, solid lines, and dashed lines) indicate the variations of neutron capture cross sections of nuclides with incident neutron energy, and dot types represent the values of natural S_n at different energies

The uncertainty arising from the experimental conditions includes variations in the energy spectrum and proton beam power, both of which directly affect the neutron flux at the target. This uncertainty is subsequently propagated into the yield through the term I in Eq.(9). According to the findings of the Back-n collaboration [27], the uncertainty associated with the energy spectrum in the Back-n ES#2 without a lead absorber ranges between 2.3 and 4.5% above 0.15 MeV and less than 8.0% below 0.15 MeV. The uncertainties stemming from the beam power are listed in Table 1. As shown in Table 1, in addition to Sm, the target material also contained trace quantities of other elements, and their contents varied from 0.001% to 0.01%. As the contents of these impurities are sufficiently low, their impact on the measurement results of the Sm neutron capture cross section is less than 1%.

Uncertainties in the data analysis were primarily attributed to the PHWT method. In 2002, Tain et al. compared the neutron-width PHWT treatment results of a 1.15 keV peak in ^{56}Fe with the experimental results, revealing a systematic error of 2.00%–3.00% [38]. This level of uncertainty can only be achieved if proper consideration is given to the threshold, conversion electrons, and γ-ray summing effects. Our simulation involved a complete reconstruction of the target and detector systems, while also incorporating a cascade γ emission program that included a model of the internal conversion processes. These efforts served to minimize additional uncertainty when applying PHWT to our results.

By contrast, the uncertainty stemming from the normalization method used to determine the absolute value of the term I in Eq. (9) affects the precision of the capture yield. The two normalization methods are provided in Refs. [26]: Gaussian fitting of one of the resonance peaks (typically, selecting the first peak in the experimental energy region for a ^{nat}Sm target which is 3.4 eV). The normalized coefficient is calculated by comparing the fitted curve with evaluation data, and CENDL-3.2 database was utilized in this study. Another approach involves comparing energy bins individually. The normalized uncertainty varies for different targets and is less than 1.3%

The ^{nat}Sm experiment was concluded in 2019, and the experimental data for the in-beam γ-ray background were unfortunately not available. Therefore, we employed the methodology outlined in Ref. [36] to analyze the in-beam γ-ray background. The uncertainty within the energy range of 20–300 eV was less than 10.5%.

The statistical uncertainty of the experiment was less than 0.68%. All error sources and their estimates are summarized in Table 2.

3.3 Neutron resonance parameters

The neutron capture yield of a natural Sm target was measured within the resonance energy range of 1–300 eV.

Table 2 Statistical error and systematic error of the experiment

σ	Meaning	Value
Experimental conditions		
σ(Beam Power)	Uncertainty from beam power	see Table 1
σ(Target)	Uncertainty from impurities in the target	< 1%
$\sigma(I_2)$	Uncertainty from energy spectra below 0.15 MeV	< 8.00%
Data analysis		
σ(PHWT)	Uncertainty from PHWT method	< 3.00%
σ(Normalized)	Uncertainty from normalized	< 1.30%
σ(In − Beam)	Uncertainty from counts of in-beam BKG	< 10.5%
Statistical error		
σ(Statistic)	Uncertainty from mathematical statistics	< 0.68%

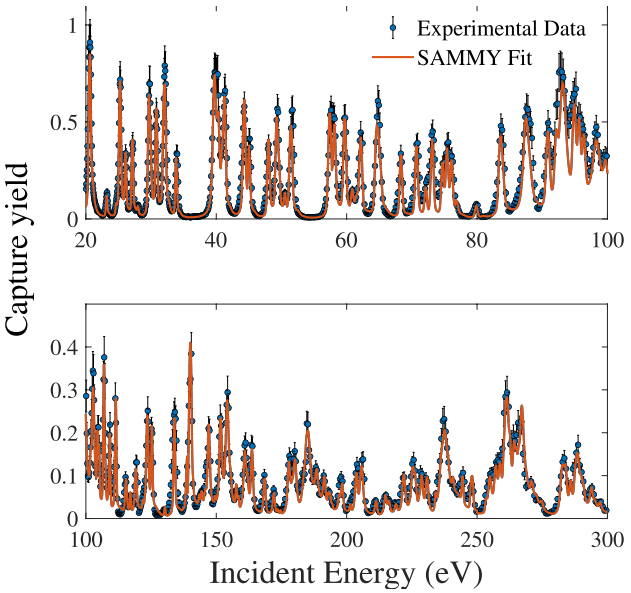

Fig. 5 (Color online) Experimental capture yields and the fitted ones obtained with the SAMMY code

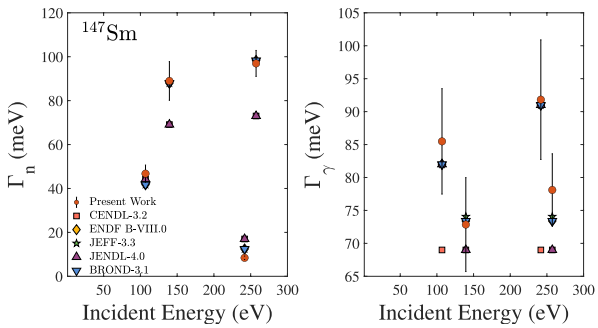

Fig. 6 (Color online) Comparison between the Γ_n and Γ_γ values of ^{147}Sm obtained from the different databases and this study

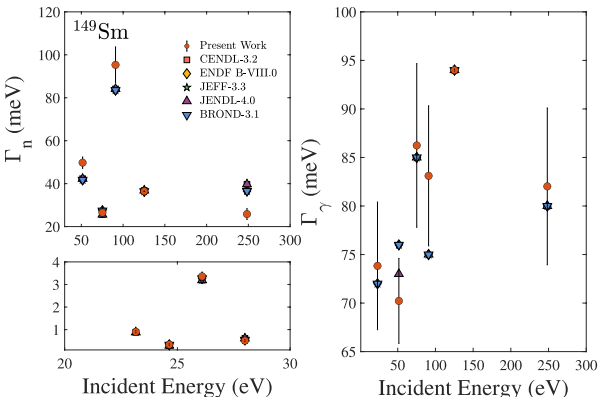

Fig. 7 (Color online) Comparison between the Γ_n and Γ_γ values of ^{149}Sm obtained from the different databases and this study

Capture yield data were obtained using Eq. 10 and subsequently fitted using the *R*-Matrix code SAMMY, accounting for various experimental effects such as Doppler broadening, self-shielding, and multiple scattering. The resonance parameters ^{nat}Sm(n,γ) were extracted accordingly. The fitting results are shown in Fig. 5. In the resonance energy region, each peak is attributed to a specific nuclide. Thus, the resonance information of each isotope can be extracted from the results of natural targets based on the resonance energy. Furthermore, Table 3 presents a detailed comparison of the differences between the different evaluation databases (DB#1-5 representing CENDL-3.2, ENDF/B-VIII.0, JEFF-3.3, JENDL-4.0, BROND-3.1).

A comparison of the findings of the current study with those of various evaluation libraries is illustrated in Fig. 6 (^{147}Sm) and Fig. 7 (^{149}Sm). For the ^{147}Sm isotope, the parameter Γ_n remains consistent at 107.0 eV across the different evaluation databases, and our experimental results agree with all of them. However, at the energy points of 139.4 eV, 241.7 eV, and 257.3 eV, the parameter Γ_n in the CENDL-3.2 database aligns with the JENDL-4.0 database but diverges from the ENDF/B-VIII.0, JEFF-3.3, and BROND-3.1 For these energy points, our experimental results were consistent with the evaluations in the ENDF/B-VIII.0, JEFF-3.3, and

Table 3 Clarification of differences between different evaluation databases

Mass	E_n (eV)	Γ_n						Γ_γ					
		Present work	DB#1	DB#2	DB#3	DB#4	DB#5	Present work	DB#1	DB#2	DB#3	DB#4	DB#5
147	107.0	46.8 ± 4.0	44.2	41.8	41.8	44.2	41.8	85.5 ± 8.0	69.0	82.0	82.0	82.0	82.0
	139.4	89.0 ± 8.8	69.1	88.0	88.0	69.1	88.0	72.9 ± 7.1	69.0	73.4	74.1	69.0	73.4
	241.7	8.4 ± 0.8	17.0	12.4	12.4	17.0	12.4	91.8 ± 9.2	69.0	91.0	91.0	91.0	91.0
	257.3	96.9 ± 6.5	73.0	98.3	98.3	73.0	98.3	78.1 ± 5.8	69.0	73.4	74.1	69.0	73.4
149	23.2	0.9 ± 0.1	0.9	7.9	7.9	0.9	7.9	73.8 ± 6.8	62.0	72.0	72.0	62.0	72.0
	24.6	0.3 ± 0.1	0.3	0.3	0.3	0.3	0.3	39.4 ± 3.9	62.0	40.0	40.0	62.0	40.0
	26.1	3.4 ± 0.3	3.2	3.3	3.3	3.2	3.3	51.7 ± 5.0	62.0	49.0	49.0	62.0	49.0
	28.0	0.5 ± 0.1	0.6	0.5	0.5	0.6	0.5	39.7 ± 4.0	62.0	40.0	40.0	62.0	40.0
	51.5	49.8 ± 3.2	42.3	41.8	41.8	42.3	41.8	70.2 ± 5.1	62.0	76.0	76.0	73.0	76.0
	75.2	26.5 ± 2.3	25.6	27.4	27.4	25.6	27.4	86.2 ± 8.4	62.0	85.0	85.0	85.0	85.0
	90.9	95.3 ± 8.8	84.1	83.6	83.6	84.1	83.6	83.1 ± 7.2	62.0	75.0	75.0	75.0	75.0
	125.3	36.4 ± 4.0	36.8	36.4	36.4	36.8	36.4	94.0 ± 9.8	62.0	94.0	94.0	94.0	94.0
	248.4	25.8 ± 2.6	39.7	36.6	36.6	39.7	36.6	82.0 ± 8.1	62.0	80.0	80.0	80.0	80.0

BROND-3.1 databases. The value of parameter Γ_γ for ^{147}Sm in the CENDL-3.2 database is 69 meV at 107 eV compared to 82 meV in the other four databases; however, our current experimental result is 85.5 ± 8.0 meV.

For the ^{149}Sm isotope, the discrepancy in the parameter Γ_n across different evaluation databases was minimal, and the experimental findings aligned closely with the assessment databases at most energy levels. Specifically, our experiment yielded a value of 25.8 ± 2.5 meV at an energy of 248.4 eV, whereas the four evaluation databases reported values ranging from 36.6 to 39.7 meV. The Γ_γ value in the CENDL-3.2 database aligns with that in the JENDL-4.0 database at the energy points 23.2, 24.6, 26.1, and 28.0 eV. However, it diverges from the evaluation databases of ENDF/B-VIII.0, JEFF-3.3, and BROND-3.1. At the energy points of 51.5, 75.2, 90.9, 125.3, and 248.4 eV, the experimental results are consistent with those in the ENDF/B-VIII.0, JEFF-3.0, JENDL-4.0, and BROND-3.1 databases.

4 Summary and conclusion

The neutron capture cross section of a natural samarium target was measured at the Back-n facility in the China Spallation Neutron Source. The environmental and neutron-scattering backgrounds were subtracted through experimental measurements, whereas the in-beam γ-ray background was removed by combining experiments and simulations. Subsequently, the neutron resonance parameters for various Sm isotopes from 20 to 300 eV were extracted using the SAMMY code based on the R-matrix theory. For the parameters Γ_n and Γ_γ in these energies of ^{147,149}Sm, the percentages consistent with the results of the CENDL-3.2, ENDF/B-VIII.0, JEFF-3.3, JENDL-4.0, and BROND-3.1 database are 27%, 65%, 65%, 42%, and 58%, respectively. However, 27% of the results were inconsistent with those of the major libraries. This work enriches experimental data of the ^{147,149}Sm neutron capture resonance and helps clarify the differences between different evaluation databases at the above energies.

Acknowledgements We appreciate the technical support provided by Dr. Yi-Jie Wang of Tsinghua University, Dr. Yu-Chao Xu of General Electric, and Dr. Xing-Yuan Xu of the University of Science and Technology of China. We thank the staff members of the Back-n white neutron facility (https://cstr.cn/31113.02.CSNS.Back-n) at the China Spallation Neutron Source (CSNS) (https://cstr.cn/31113.02.CSNS), for providing technical support and assistance in data collection and analysis. We thank Hunan WeiYu Network Technology Co., Ltd., for providing technical support.

Author contributions All authors contributed to the study conception and design. Material preparation, data collection, and analysis were performed by Xin-Xiang Li, Hong-Wei Wang, and Wen Luo. The first draft of the manuscript was written by Xin-Xiang Li, and all authors commented on previous versions of the manuscript. All authors read and approved the final manuscript.

Data availability The data that support the findings of this study are openly available in Science Data Bank at https://cstr.cn/31253.11.sciencedb.25404. and https://www.doi.org/10.57760/sciencedb.25404.

Declarations

Conflict of interest Hong-Wei Wang and Chun-Wang Ma are the editorial board member for Nuclear Science and Techniques and were not involved in the editorial review, or the decision to publish this article. All authors declare that there is no conflict of interest.

References

1. F. Käppeler, R. Gallino, S. Bisterzo et al., The s process: nuclear physics, stellar models, and observations. Rev. Mod. Phys. **83**, 157–193 (2011). https://doi.org/10.1103/RevModPhys.83.157
2. J.J. Cowan, F.K. Thielemann, The r-process and nucleochronology. Phys. Rep. **208**, 267–394 (1991). https://doi.org/10.1016/0370-1573(91)90070-3
3. M. Arnould, S. Goriely, The p-process of stellar nucleosynthesis: astrophysics and nuclear physics status. Phys. Rep. **384**, 1–84 (2003). https://doi.org/10.1016/S0370-1573(03)00242-4
4. Y.E. Penionzhkevich, Nuclear astrophysics. Phys. Atom. Nucl. **73**, 1460–1468 (2010). https://doi.org/10.1134/S106377881008020X
5. C.X. Tan, X.X. Li, D.Y. Pang et al., ^{233}Pa (n,γ) cross section extraction using the surrogate reaction ^{232}Th(^{3}He, p)^{234}Pa* involving spin-parity distribution. Phys. Rev. C **109**, 044615 (2024). https://doi.org/10.1103/PhysRevC.109.044615
6. H.H. Xiong, Q.S. Zeng, Y.C. Han et al., Neutronics analysis of a subcritical blanket system driven by a gas dynamic trap-based fusion neutron source for ^{99}Mo production. Nucl. Sci. Tech. **34**, 49 (2023). https://doi.org/10.1007/s41365-023-01206-2
7. H. Chen, X.L. Wang, China's first pulsed neutron source. Nat. Mater. **15**, 689–691 (2016). https://doi.org/10.1038/nmat4655
8. B. Jiang, B.B. Tian, H.T. Jing et al., Feasibility of medical radioisotope production based on the proton beams at China Spallation Neutron Source. Nucl. Sci. Tech. **35**, 102 (2024). https://doi.org/10.1007/s41365-024-01438-w
9. J. Xue, S. Feng, Y.H. Chen et al., Measurement and analysis of the neutron-induced total cross-sections of ^{209}Bi from 0.3 eV to 20 MeV on the Back-n at CSNS. Chin. Phys. C. **47**, 124001 (2023). https://doi.org/10.1088/1674-1137/acf920
10. G.L. Yang, Z.D. An, W. Jiang et al., Measurement of Br(n,γ) cross sections up to stellar s-process temperatures at the CSNS Back-n. Nucl. Sci. Tech. **34**, 180 (2023). https://doi.org/10.1007/s41365-023-01337-6
11. S. Wang, S.X. Fang, S.N. Fu et al., Introduction to the overall physics design of CSNS accelerators. Chin. Phys. C **33**, 1 (2009). https://doi.org/10.1088/1674-1137/33/S2/001
12. S. Wang, Y.W. An, S.X. Fang et al., An overview of design for CSNS/RCS and beam transport. Sci. China, Ser. G **54**, 239–244 (2011). https://doi.org/10.1007/s11433-011-4564-x
13. T.R. Liang, Z.D. Li, W. Yin et al., Simulation of a high energy neutron irradiation facility at beamline 11 of the China spallation neutron source. Nucl. Instrum. Meth. A **860**, 24–28 (2017). https://doi.org/10.1016/j.nima.2017.04.004
14. H. Liu, J. Peng, K. Gong et al., Design and construction of CSNS drift tube linac. Nucl. Instrum. Meth. A **911**, 131–137 (2018). https://doi.org/10.1016/j.nima.2018.10.034
15. L. Zhu, J.R. Zhou, Y.G. Xia et al., Large area ^{3}He tube array detector with modular design for multi-physics instrument at CSNS. Nucl. Sci. Tech. **34**, 1 (2023). https://doi.org/10.1007/s41365-022-01161-4
16. Q. Li, G.Y. Luan, J. Bao et al., The ^{6}LiF-silicon detector array developed for real-time neutron monitoring at white neutron beam at CSNS. Nucl. Instrum. Meth. A **946**, 162497 (2019). https://doi.org/10.1016/j.nima.2019.162497
17. R. Fan, H. Jiang, W. Jiang et al., Detection of low-energy charged-particle using the ΔE-E telescope at the Back-n white neutron source. Nucl. Instrum. Meth. A **981**, 164343 (2020). https://doi.org/10.1016/j.nima.2020.164343
18. S. Zhang, G. Li, W. Jiang et al., Measurement of the ^{159}Tb(n,γ) cross section at the CSNS Back-n facility. Phys. Rev. C **107**, 045809 (2023). https://doi.org/10.1103/PhysRevC.107.045809
19. H.Y. Jiang, W. Jiang, Z. Cui et al., Measurement of the relative differential cross sections of the ^{1}H (n, el) reaction in the neutron energy range from 6 MeV to 52 MeV. Eur. Phys. J. A **57**, 6 (2021). https://doi.org/10.1140/epja/s10050-020-00313-7
20. D.J. Zhao, S. Feng, P.J. Cheng et al., Conceptual design of a $Cs_2LiLaBr_6$ scintillator-based neutron total cross section spectrometer on the Back-n beam line at CSNS. Nucl. Sci. Tech. **34**, 3 (2023). https://doi.org/10.1007/s41365-022-01152-5
21. J.Y. Tang, Q. An, J.B. Bai et al., Back-n white neutron source at CSNS and its applications. Nucl. Sci. Tech. **32**, 11 (2021). https://doi.org/10.1007/s41365-021-00846-6
22. R.R. Fan, Q. Li, J. Bao et al., Detector development at the Back-n white neutron source. Radiation-detection technology and methods. **7**, 171–191 (2023). https://doi.org/10.1007/s41605-022-00379-5
23. X.X. Li, L.X. Liu, W. Jiang et al., Experimental determination of the neutron resonance peak of ^{162}Er at 67.8 eV. Phys. Rev. C **106**, 065804 (2022). https://doi.org/10.1103/PhysRevC.106.065804
24. J. Ren, X. Ruan, J. Bao et al., The C_6D_6 detector system on the Back-n beam line of CSNS. Radiat.-Detect. Technol. Methods **3**, 52 (2019). https://doi.org/10.1007/s41605-019-0129-8
25. X.R. Hu, G.T. Fan, W. Jiang et al., Measurements of the ^{197}Au(n,γ) cross section up to 100 keV at the CSNS Back-n facility. Nucl. Sci. Tech. **32**, 101 (2021). https://doi.org/10.1007/s41365-021-00931-w
26. X.X. Li, L.X. Liu, W. Jiang et al., New experimental measurement of ^{nat}Er(n, γ) cross sections between 1 and 100 eV. Phys. Rev. C **104**, 054302 (2021). https://doi.org/10.1103/PhysRevC.104.054302
27. Y.H. Chen, G.Y. Luan, J. Bao et al., Neutron energy spectrum measurement of the Back-n white neutron source at CSNS. Eur. Phys. J. A **55**, 115 (2019). https://doi.org/10.1140/epja/i2019-12808-1
28. J.C. Wang, J. Ren, W. Jiang et al., In-beam gamma rays of CSNS Back-n characterized by black resonance filter. Nucl. Sci. Tech. **35**, 164 (2024). https://doi.org/10.1007/s41365-024-01553-8
29. B. Jiang, J.L. Han, W. Jiang et al., Monte-Carlo calculations of the energy resolution function with Geant4 for analyzing the neutron capture cross section of ^{232}Th measured at CSNS Back-n. Nucl. Instrum. Meth. A **1013**, 165677 (2021). https://doi.org/10.1016/j.nima.2021.165677
30. X.Y. Liu, Y.W. Yang, R. Liu et al., Measurement of the neutron total cross section of carbon at the Back-n white neutron beam of CSNS. Nucl. Sci. Tech. **30**, 139 (2019). https://doi.org/10.1007/s41365-019-0660-9
31. H. Yi, T.F. Wang, Y. Li et al., Double-bunch unfolding methods for back-n white neutron source at CSNS. J. Instrum. **15**, 03 (2020). https://doi.org/10.1088/1748-0221/15/03/P03026
32. R.L. Macklin, J.H. Gibbons, ^{208}Pb(n, γ) cross sections by activation between 10 and 200 keV. Phys. Rev. **181**, 1639 (1969). https://doi.org/10.1103/PhysRev.181.1639
33. B. Jiang, J.L. Han, J. Ren et al., Measurement of ^{232}Th(n,γ) cross section at the CSNS Back-n facility in the unresolved resonance region from 4 keV to 100 keV. Chin. Phys. B **31**, 060101 (2022). https://doi.org/10.1088/1674-1056/ac5394
34. S. Agostinelli, J. Allison, K. Amako et al., Geant4-a simulation toolkit. Nucl. Instrum. Meth. A **506**, 250–303 (2003). https://doi.org/10.1016/S0168-9002(03)01368-8
35. X.M. Shi, G.L. Wang, K.J. Luo et al., Geant4 development for actinides photofission simulation. Nucl. Instrum. Meth. A **1062**, 169222 (2024). https://doi.org/10.1016/j.nima.2024.169222
36. X.X. Li, L.X. Liu, W. Jiang et al., Measurements of the ^{107}Ag neutron capture cross sections with pulse height weighting

technique at the CSNS Back-n facility. Chin. Phys. B **31**, 038204 (2022). https://doi.org/10.1088/1674-1056/ac48fd
37. W.J. Huang, M. Wang, F.G. Kondev et al., The AME 2020 atomic mass evaluation (I). Evaluation of the input data and adjustment procedures. Chin. Phys. C. **45**, 030002 (2021). https://doi.org/10.1088/1674-1137/abddb0
38. J.L. Tain, F. Gunsing, D. Aniel-Cano et al., Accuracy of the pulse height weighting technique for capture cross section measurements. J. Nucl. Sci. Technol. **39**, 689–692 (2002). https://doi.org/10.1080/00223131.2002.10875193

Authors and Affiliations

Xin-Xiang Li[1] · Long-Xiang Liu[2] · Wei Jiang[3,4] · Ya-Ju Chen[1] · Jie Ren[5] · Hong-Wei Wang[2,6] · Gong-Tao Fan[2,6] · Wen Luo[1] · Song Feng[1] · Wen Xie[1] · Zi-Ang Lin[1] · Ting Jiang[1] · Gao-Le Yang[7] · Zhen-Dong An[8] · Xian-Kai Li[1,7] · Zhou-Ji Liao[1] · Jie-Ming Xue[9] · Xin-Yu Li[10] · Ning-Xin Peng[1] · De-Xin Wang[11] · Su-Ya-La-Tu Zhang[11] · Yue Zhang[2] · Xin-Rong Hu[12] · Zi-Rui Hao[2] · Bing Jiang[3,4] · Xiao-He Wang[13] · Ji-Feng Hu[13] · Ying-Du Liu[14] · Chun-Wang Ma[15,16] · Yu-Ting Wang[15] · Jian-Jun He[17] · Li-Yong Zhang[18,19]

✉ Xin-Xiang Li
lixinxiang@usc.edu.cn

✉ Hong-Wei Wang
wanghw@sari.ac.cn

✉ Wen Luo
wenluo-ok@163.com

1 School of Nuclear Science and Technology, University of South China, Hengyang, China

2 Shanghai Advanced Research Institute, Chinese Academy of Sciences, Shanghai, China

3 Institute of High Energy Physics, Chinese Academy of Sciences, Beijing 100049, China

4 China Spallation Neutron Source, Dongguan 523803, China

5 China Institute of Atomic Energy, Beijing 102413, China

6 University of Chinese Academy of Sciences, Beijing 100049, China

7 Sun Yat-sen University, Zhuhai 510275, China

8 Institute of Modern Physics, Chinese Academy of Sciences, Lanzhou 730000, China

9 Key Laboratory of Nuclear Data, China Institute of Atomic Energy, Beijing 102413, China

10 School of Microelectronics and Communication Engineering, Chongqing University, Chongqing 401331, China

11 College of Mathematics and Physics, Inner Mongolia Minzu University, Tongliao 028000, China

12 Chengdu University of Technology, Chengdu 610059, China

13 Shanghai Institute of Applied Physics, Chinese Academy of Sciences, Shanghai 201800, China

14 Xiangtan University, 411105 Xiangtan, China

15 Henan Normal University, Xinxiang 453007, China

16 Institute of Nuclear Science and Technology, Henan Academy of Sciences, Zhengzhou 450015, China

17 Fudan University, Shanghai 200433, China

18 Key Laboratory of Beam Technology and Material Modification of Ministry of Education, College of Nuclear Science and Technology, Beijing Normal University, Beijing 100875, China

19 Beijing Radiation Center, Beijing, China